CSIRO PUBLISHING

Exploration Geophysics
http://dx.doi.org/10.1071/EG12008

Global optimisation by simulated annealing for common reflection surface stacking and its application to low-fold marine data in southwest Japan

Shohei Minato[1,4] Takeshi Tsuji[1] Toshifumi Matsuoka[1] Naoki Nishizaka[2] Michiharu Ikeda[3]

[1]Kyoto University, Graduate School of Engineering, C1 Kyoto-Daigaku Katsura, Nishikyo-ku, Kyoto 6158540, Japan.
[2]Shikoku Electric Power Co. Inc., Marunouchi 2-5, Takamatsu, Kagawa, 7608573, Japan.
[3]Shikoku Research Institute Inc., Yashimanishimachi 2109, Takamatsu, Kagawa, 7610192, Japan.
[4]Corresponding author. Email: s_minato@earth.kumst.kyoto-u.ac.jp

Abstract. The common reflection surface (CRS) stack is an alternative method of producing a zero-offset stacked section with a higher signal-to-noise ratio (SNR) than the conventional normal moveout (NMO)/dip moveout (DMO) stack method. Since, however, it is difficult to determine global optimal parameters for the CRS stack method by the conventional three-step search method, especially for complex structures and low-fold data, we investigate the ability of simulated annealing (SA) to optimise our estimation of these parameters. We show a detailed but practical procedure for the application of SA to the CRS stack method. We applied the CRS stack method with SA to numerically modelled seismic reflection data, and to multichannel marine seismic data over complicated geological structures around the Median Tectonic Line (MTL) in Japan. We used the results of the conventional three-step search algorithm as the initial model for the SA search and showed that with this approach SA can estimate CRS parameters accurately within a reasonable number of calculations. The CRS stack method with this approach provided a clearer seismic profile with a higher SNR than either a conventional NMO stack method or a conventional CRS stack method.

Key words: common reflection surface, Median Tectonic Line, simulated annealing.

Received 17 January 2012, accepted 21 January 2012, published online 1 March 2012

Introduction

Stacking of common midpoint gathers (CMPs) from multifold seismic reflection data to provide a zero-offset (ZO) section has traditionally been used to image subsurface structures. The conventional normal moveout (NMO) stack uses a stacking operator that is a hyperbolic function for each CMP gather, assuming a horizontally layered earth. On the other hand, the common reflection surface (CRS) stack method (Müller, 1999; Jäger et al., 2001; Mann, 2002) is categorised as one of the multi-parameter stacking techniques (e.g. multifocusing, Gelchinsky, 1989, Gelchinsky et al., 1999; polystack, Thore et al., 1994). It has been reported that the CRS stack method provides higher signal-to-noise ratios (SNR) than conventional NMO/DMO stacking for low-quality data acquired, for example, in sedimentary environments during hydrocarbon exploration (Trappe et al., 2001; Bergler et al., 2002) or in deep seismic crustal imaging (Menyoli et al., 2004; Yoon et al., 2009). The differences between the CRS stack method and conventional NMO stack method are: (i) the CRS stack does not explicitly require a macrovelocity model; and (ii) fold numbers in the CRS stack method can become higher than in the NMO stack method. The CRS stacking parameters are derived fully automatically from the prestack seismic data volume. These CRS parameters can be used to estimate subsurface interval velocities (Duveneck, 2004) and to enhance, interpolate, and extrapolate trace data (Baykulov and Gajewski, 2009).

Just as a conventional NMO stack requires accurate stacking velocities, CRS analysis requires reliable estimation of the CRS parameters. A 2D CRS stacking operator is defined by three parameters at each ZO point (CMP and time) of the ZO section: the emergence angles of reflected waves, α, and two radii of eigenwaves, R_N, R_{NIP} (Hubral, 1983). These three CRS parameters are determined by a parameter-search algorithm, using semblance of the traces. The algorithm searches for the CRS parameters that produce the most coherent CRS stacked section from the prestack seismic data volume. This is a 3D optimisation problem. However, solving 3D optimisation problems for all the ZO points is highly time-consuming. Therefore, in general, a three-step search algorithm has been adopted for this purpose. It contains three 1D optimisation steps (e.g. Jäger et al., 2001) and searches for the CRS parameters in the NMO stacked section, assuming that the conventional NMO stacked section approximates a ZO section. Therefore, optimal CRS parameters are obtained only if the NMO stacked section is a good approximation of a ZO section, as is the case for high-fold data. However, the accuracy of the CRS parameters and the quality of the resultant CRS stacked section are compromised if the NMO stacked section is inaccurate because of, for example, complex structures or low fold. Therefore, implementing a simultaneous 3D search must be considered in order to apply the CRS stack method to such data.

The first proposed 3D optimisation is the so-called Flexible Polyhedron search (Jäger et al., 2001). This method is applied after a three-step search, and designs a polyhedron with four vertices in the 3D parameter domain and sequentially compares them to get to a point with higher coherence (Nelder and Mead, 1965). Müller (2003) modified this method by introducing the Metropolis criterion of Simulated Annealing (SA) in order to have the ability to escape from local solutions. Garabito et al. (2001) first applied SA to search directly for the CRS parameters, after simplifying them into two parameters by considering only diffraction in the CRS stacking operator. Garabito et al. (2006, 2009) further applied SA to search directly for the three CRS parameters. Note that Garabito et al. (2006) uses randomly created initial models and therefore multiple trials should be performed in order to get the highest coherence. Bonomi et al. (2009) implemented conjugate-gradient optimisation especially for the 3D CRS stack method.

The direct search for three CRS parameters using SA (e.g. Garabito et al., 2006) is the most time-consuming option among the simultaneous optimisations described above. However, the advantages of SA over other simultaneous searching methods are that: (i) it is still affordable if the amount of data is not very large; (ii) it does not use gradient information; and (iii) it is less dependent on the initial model than local-optimisation methods such as the steepest-descent method (Sen and Stoffa, 1995). Since the function to be optimised for the CRS stack method (coherence) is multimodal and its derivative information is available only numerically, we can use the SA method to acquire a global solution with less dependence on initial parameters. Furthermore, if data are low-fold and the computational cost is inexpensive, SA can be the best choice.

For this paper we have applied the CRS stack method to delineate the Median Tectonic Line (MTL) of south-west Japan. The MTL is the most significant fault in Japan, extending ~1000 km approximately NE–SW across Honshu, Shikoku, and Kyushu Islands. The western segment of the MTL is an active right-lateral strike-slip fault. Understanding the detailed subsurface geological structure around the MTL becomes important for earthquake hazard prevention. The seismic data were acquired along a line normal to the coastline. The survey area is close to the coast in an area of heavy ship traffic, and we could not tow a sufficiently long streamer cable. Consequently, the data are low-fold, so we apply simultaneous 3D optimisation using SA to the data.

Although simultaneous optimisation for the CRS stack method has been investigated by several authors, it is hard to find a well organised and readable article. In this paper, therefore, we follow the simultaneous optimisation approach step by step, using numerical data and field data.

Method

CRS stacking operator

For multifold seismic reflection data, the CRS stack method produces a ZO section by using a stacking surface operator. In the vicinity of a particular midpoint (x_0), the stacking operator for the ZO traveltime (t_0) is described by the following equation

$$t^2(x_m,h)=\left(t_0+\frac{2\sin\alpha}{v_0}(x_m-x_0)\right)^2+\frac{2t_0\cos^2\alpha}{v_0}\left(\frac{(x_m-x_0)^2}{R_N}+\frac{h^2}{R_{NIP}}\right) \quad (1)$$

Here, v_0 is surface velocity, x_m is the midpoint around x_0, and h is the half offset. Equation 1 is the second-order Taylor approximation of traveltime for a common reflection point (CRP) trajectory in an arbitrary medium (Höcht et al., 1999) and this traveltime is characterised by three parameters (α, R_N, R_{NIP}) for the CRS stack. These parameters describe a local reflector segment and can be explained by two hypothetical experiments (Figure 1) as follows.

Let us consider the seismic response from a point reflector in the subsurface (Figure 1*a*) by assuming that the observed reflected waves originated from the point reflector. We define α as the emergence angle of a reflection ray reaching a given midpoint x_0, and R_{NIP} as the radius of the corresponding wavefront, approximating it to be circular. We consider an explosive reflector experiment (Figure 1*b*) in order to take into account the shape of the local reflector segment. We have the same emergence angle and again define R_N as the radius of the wavefront. Therefore, R_N is a parameter that describes the curvature of the local reflector segment. A detailed discussion of the CRS stacking operator is provided by Hubral (1983) and Jäger et al. (2001).

From equation 1, the CRS stacking operator forms a surface in the (x_m, h) domain, thus the number of traces increases to contribute to the subsurface imaging compared to a conventional NMO stack. Furthermore, the CRS stack does not explicitly require a macrovelocity model, but does need the surface velocity v_0. If we substitute $x_m = x_0$ in equation 1, we have

$$t^2(h)=t_0^2+\frac{2t_0\cos^2\alpha}{v_0}\frac{h^2}{R_{NIP}} \quad (2)$$

which is a half-offset hyperbolic stacking operator and is therefore identical to the NMO stacking operator with a stacking velocity

$$V_{stack}^2=\frac{2v_0R_{NIP}}{t_0\cos^2\alpha} \quad (3)$$

Three-step search algorithm

The CRS stack method requires a search for appropriate CRS parameters (α, R_N, R_{NIP}) for every ZO point. This search is based on coherency analysis (Neidell and Taner, 1971). Different sets of the CRS parameters are evaluated to find the combination that gives the highest coherency of signals along the CRS stacking

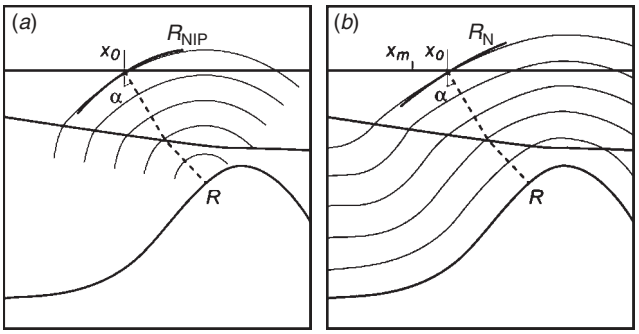

Fig. 1. Schematic diagram showing eigenwaves and CRS parameters (modified after Jäger et al., 2001). (*a*) Eigenwaves for a point source at R. x_0 is a ZO point and α indicates the emergence angle of the central ray at x_0. R_{NIP} is the radius of curvature of the circle that approximates the wavefront near x_0. (*b*) Eigenwaves for an exploding reflector near R. x_m is in the vicinity of the ZO point x_0, and α indicates the emergence angle of the central ray at x_0. R_N is the radius of curvature of the circle that approximates the wavefront near x_0.

surface in the prestack data volume. High coherence indicates that the recorded reflection events are well approximated by the CRS stacking operator. Coherence S is defined as

$$S(\alpha, R_{NIP}, R_N; x_0, t_0) = \frac{\sum_{j=k(i)-w/2}^{k(i)+w/2}\left(\sum_{i=1}^{M} f_{i,j(i)}\right)^2}{M\sum_{j=k(i)-w/2}^{k(i)+w/2}\sum_{i=1}^{M} f_{i,j(i)}^2} \quad (4)$$

where $f_{i,j}$ is the amplitude of the j-th time sample at the i-th trace among M traces that are used for the CRS stack, and $k(i)$ is the traveltime of the CRS stack operator for the i-th trace. The summation of j is performed to provide a window around the CRS parameters. The length of the window (w) should approximate the wavelength of the seismic signal. Coherence values range from 0 to 1, where 1 indicates the highest coherence.

The simultaneous search for the three CRS parameters becomes a 3D optimisation problem. However, it is commonly implemented as three separate cascaded processes of 1D optimisation (three-step search algorithm): 'automatic CMP stack', followed by 'linear ZO stack' and 'hyperbolic ZO stack' (Jäger et al., 2001; Müller, 2009).

The automatic CMP stack is a conventional NMO stack (equation 2) and searches for the stacking velocity (V_{stack}, equation 3) giving the highest coherence S. The linear ZO stack searches for the emergence angle (α) in the NMO stacked section (approximating the ZO section) assuming linear reflectors. For a linear reflector ($R_N = \infty$) the CRS stacking operator in the ZO section ($h = 0$) can be written as

$$t(x_m) = t_0 + \frac{2\sin\alpha}{v_0}(x_m - x_0) \quad (5)$$

The discretised values of α are tested to find the value that gives the highest coherency in the NMO stacked section. The values of V_{stack} and α obtained are then used to calculate R_{NIP} using equation 3. Finally, the hyperbolic ZO stack searches for the radius of the normal wave (R_N) with the given emergence angle (α). The CRS stacking operator for the ZO section ($h = 0$) is

$$t^2(x_m, h) = \left(t_0 + \frac{2\sin\alpha}{v_0}(x_m - x_0)\right)^2 + \frac{2t_0\cos^2\alpha}{v_0}\frac{(x_m - x_0)^2}{R_N} \quad (6)$$

The emergence angle estimated from the linear ZO stack is used in equation 6 to find the value of R_N giving the highest coherency in the NMO stacked section. The CRS parameters so obtained are then used for CRS stacking (equation 1).

SA optimisation of CRS parameters

The cascaded three-step search algorithm is less time-consuming than a 3D optimisation algorithm, but it requires a high-quality initial NMO stacked section. The accuracy of the CRS parameters and the quality of the CRS stacked sections derived using this algorithm are reduced when the seismic data is low-fold or complex structures exist that do not satisfy the assumption of a horizontally layered earth. In such cases a 3D optimisation algorithm is required to obtain clear subsurface images. Because the function to be optimised (equation 4) is known to be a multimodal function that has multiple local maxima (Jäger et al., 2001), we tested the application of SA to optimise the CRS parameters.

SA is an optimisation method based on probability theory (Kirkpatrick et al., 1983) that borrows its basic concept from the physical annealing process, in which a more stable crystal structure with lower energy may be obtained when a material is heated or reheated and slowly cooled from a high temperature. This method has been useful in many geophysical applications (e.g. Rothman, 1985; Sen and Stoffa, 1995; Velis and Ulrych, 1996).

SA can search for model parameters $\mathbf{m}$ that minimise an arbitrarily defined 'energy' function $E(\mathbf{m})$. For the CRS stack method, the model parameters $\mathbf{m}$ are the CRS parameters (α, R_N, R_{NIP}) and the energy function $E(\mathbf{m})$ is defined as negative coherence S (equation 4) as follows.

$$E(\mathbf{m}) = -S(\mathbf{m}; x_0, t_0), \quad \mathbf{m} = (\alpha, R_{\mathrm{NIP}}, R_N) \quad (7)$$

SA perturbs the present model parameters $\mathbf{m}_0$ using random numbers and produces the next model parameters $\mathbf{m}_1$. The energy perturbation ΔE of this procedure is defined as

$$\Delta E = E(\mathbf{m}_1) - E(\mathbf{m}_0) \quad (8)$$

If $\Delta E \leq 0$, the new model is always accepted. If $\Delta E > 0$, the new model is accepted with the probability, P, defined as

$$P = \exp\left(-\frac{\Delta E}{T}\right) \quad (9)$$

where T is temperature. This is known as the Metropolis criterion, and introducing this rule makes it possible to escape from a local minimum in E. A large value of T in equation 9 indicates a high possibility for transition towards a state with higher energy. T is set to gradually decrease as iterations proceed. At the limit as $T \to 0$, SA reduces to a simple local optimisation. If T is lowered too fast, SA cannot search sufficient model space and the model parameters are trapped into a local solution. In our research, we use the following exponential function for cooling (Sen and Stoffa, 1995):

$$T_k = T_0\exp(-Ck^{1/DIM}) \quad (10)$$

where DIM indicates the dimension of the model parameter, T_0 is the initial temperature, and C is a constant parameter that tunes the cooling rate. The Metropolis criterion makes possible an escape from local minima, so the model parameter set obtained using this function becomes the global solution derived from the initial model. Therefore, it is important to select an appropriate initial temperature T_0 and cooling rate C. If the initial temperature is too low or the cooling rate is too fast, it is difficult to escape from local minima. On the other hand, if the initial temperature is high and the cooling rate is low, a huge number of iterations may be required to achieve convergence of the energy. The appropriate values of T_0 and C are dependent on the shape of the energy function $E(\mathbf{m})$, and it is common to select them empirically (Sen and Stoffa, 1995).

The procedure of search for the CRS parameters is as follows. We consider the k-th iterative search and perturb the CRS parameters according to the following equation:

$$\mathbf{m}_k = \mathbf{m}_{k-1} + \beta_i(\mathbf{m}_{\max} - \mathbf{m}_{\min}), \quad \beta_i \in [-1, 1] \quad (11)$$

where $\mathbf{m}_{\max}$ and $\mathbf{m}_{\min}$ are the maximum and minimum values of each CRS parameter. The random number β_i is calculated from a uniformly-distributed random number u_i and temperature T_i as follows:

$$\beta_i = \mathrm{sgn}(u_i - 0.5)T_i\left[\left(1 + \frac{1}{T_i}\right)^{|2u_i - 1|} - 1\right], \quad u_i \in [-1, 1] \quad (12)$$

Equations 11 and 12 indicate that the step length for model perturbation tends to decrease with temperature. This procedure is known as Very Fast Simulated Annealing (VFSA; Ingber, 1989) and provides a faster energy convergence than conventional SA. We designed our CRS stacking operator using $\mathbf{m}_k$ (equation 11), calculated the energy perturbation ΔE from equation 8, and applied the acceptance rule of equation 9.

Application to numerical modelling

Numerical data

We numerically simulated the wavefield of a simple two-layer model (Figure 2*a*) to create a test dataset. We calculated the acoustic wavefield using a second-order finite difference acoustic wave equation. We show the modelling parameters in Table 1. The sources and receivers were located 1 m below the upper boundary of the model, which was the free surface. We show the calculated true ZO section in Figure 2*b*. We prepared seismic data comprising 401 CMPs at 5 m intervals with a maximum fold of 7. The numerical data were contaminated by Gaussian noise after eliminating direct arrivals (Figure 3).

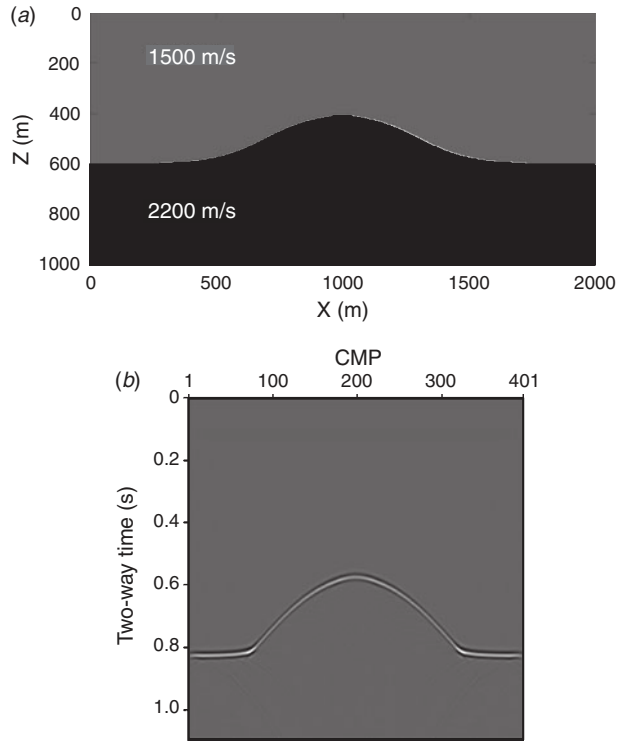

Fig. 2. (*a*) Two-layered velocity model used for numerical modelling in this study. (*b*) True (computed) ZO section without noise.

Table 1. Modelling and data parameters for the numerical modelling test.

Grid size	1 m
Record length	1.1 s
Sampling rate	1 ms
Source wavelet	Ricker
Central frequency	45 Hz
Number of CMPs	401
CMP interval	5 m
Minimum/Maximum offset	0 m/600 m
Maximum fold	7

Three-step search algorithm

For the three-step search of our CRS analysis we used a window length (w) of 0.05 s for coherence calculation (equation 4), and automatic CMP stack searches for stacking velocity V_{stack} were accomplished using equations 2 and 3. We searched for the stacking velocity in 3 m/s steps within a range from 50 m/s below to 250 m/s above the given root-mean-square (RMS) velocity of the model. The NMO stacked section (Figure 4) is noisy because of the low fold of the CMP gathers (maximum 7-fold).

Both the linear ZO stack (equation 5) and the hyperbolic ZO stack (equation 6) require the definition of an aperture in the CMP direction (the ZO aperture) to calculate the stacking operator. We used a ZO aperture of 100 m for both the linear and hyperbolic stacks of our dataset; that is, stacking was carried out only for values of x_m for which $|x_m - x_0| \leq 100$ in equations 5 and 6.

We applied a linear ZO stack and searched for the emergence angle α over a range from $-30°$ to $+30°$ with a 0.5-degree step

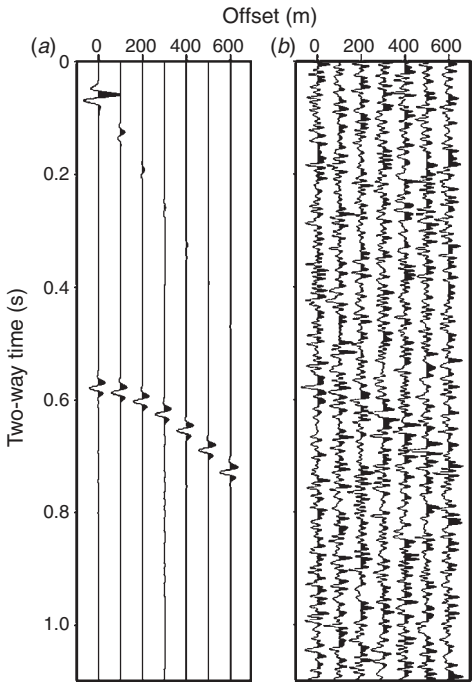

Fig. 3. Numerically modelled 7-fold CMP gather at CMP 200 (*a*) without noise and (*b*) with Gaussian noise.

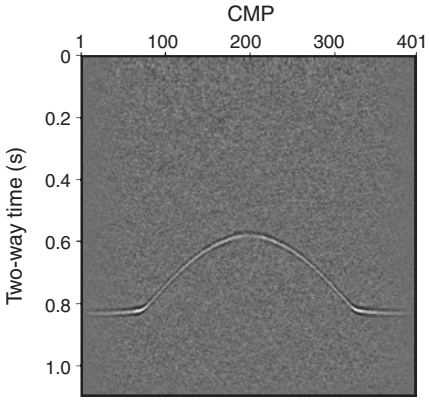

Fig. 4. NMO stacked section of the modelled data, using automatic CMP stacking.

size, and used the values obtained for α and V_{stack} in equation 3 to estimate R_{NIP}. We estimated R_N by hyperbolic ZO stacking, using α and equation 6. We then applied equation 1 using these CRS parameters and the same ZO aperture (100 m) as used for the linear and hyperbolic stacks to produce a CRS stacked section (Figure 5).

Because of its higher fold, the CRS stacked section contains less white noise than the NMO stacked section (Figure 4). However, discontinuities along the reflector in the CRS stacked section shows that the CRS parameters obtained from the three-step search did not achieve the best global solution. For example, the transition from a near-horizontal structure to dipping structure around CMP 300–400 is discontinuous because we assumed a linear reflector for our estimation of the emergence angle α. The high-frequency noise on other parts of the reflector is caused by the inaccurate V_{stack} values determined from automatic CMP stacking of low-fold data.

Search range of CRS parameters in SA optimisation

To apply the CRS stack method using SA, we must define a search range for the CRS parameters ($\mathbf{m}_{\max}$ and $\mathbf{m}_{\min}$ in equation 11). The search range we used for α was the same as that used for the linear ZO stack (−30° to +30°), and R_N ranged from −∞ to +∞ and was transformed by the following equation (Mann, 2002):

$$\gamma = \arctan\left(\frac{R_S}{R_N}\right) \tag{13}$$

where R_S is an arbitrary value (100 in this case) and γ lies in the range from −90° to +90° for R_N ranging from −∞ to +∞. For SA optimisation, we searched for an optimal value of γ defined by equation 13 instead of R_N. Finally, R_{NIP} was related to the emergence angle α and the conventional stacking velocity (V_{stack} from equation 3). Therefore, we defined the search range for R_{NIP} by applying the search range of the stacking velocity together with that of α, as described above. Multiple reflections have lower stacking velocities than neighbouring primary reflections; therefore these can be suppressed by limiting the search range for stacking velocity. The search range of R_{NIP} was calculated as follows:

$$\begin{aligned} R_{NIP}^{(\min)} &= \frac{t_0}{2v_0}\min(\cos^2\alpha)\left(V_{\text{stack}}^{(\min)}\right)^2 \\ R_{NIP}^{(\max)} &= \frac{t_0}{2v_0}\max(\cos^2\alpha)\left(V_{\text{stack}}^{(\max)}\right)^2 \end{aligned} \tag{14}$$

where the stacking velocity is constrained for each ZO point (x_0, t_0).

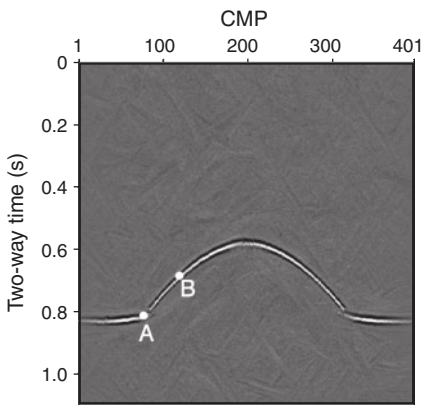

Fig. 5. CRS stacked section of the modelled data, using a conventional three-step search for stacking parameters.

The function to be optimised (equation 7) tends to decrease as the number of traces M (number of fold) decreases; that is, the coherence is higher when the number of fold is low (Mann, 2002). Depending on the combination of CRS parameters, the number of fold can change in the SA process because the algorithm seeks access to non-existent data outside the recording time. Therefore, we added the following new constraint on fold during the CRS parameter search. When the CRS parameters, perturbed by a random number, produced a fold number less than 80% of the initial fold, we discarded those parameters and selected a new set.

Initial model in SA optimisation

We need an initial model to start applying SA. To investigate the influence of the initial model on the SA search, we applied SA optimisation at ZO point A in Figure 5 (CMP 77 and two-way time = 0.802 s) using different initial models. In the SA optimisation process here, we used the exponential temperature function in equation 10, substituting $DIM = 3$, with (T_0, C) = (0.003, 0.50). We used 500 temperature values and updated the CRS parameters twice for each temperature, giving 1000 forward calculations (CRS stacking). We created 10 random initial models with the CRS parameters within the search ranges described above. In Figure 6 we compare the energy evolution from these different initial models during the SA search. The dotted lines show the energy convergence from each initial model, and the solid line shows the energy convergence using an initial model determined from the three-step search algorithm. Observe that the value of the energy at the first iteration of the solid line ($E = -0.028$) corresponds to the minimum value obtained by the conventional three-step search algorithm. The SA method successfully reached a lowest energy around $E = -0.162$ after 1000 iterations — this value is lower than that found by the three-step search. This demonstrates that SA can obtain better CRS parameters than the three-step search algorithms.

However, one can see that three of random models were trapped into local minima and never reached the global minimum (Figure 6). This observation indicates that for randomly created initial models, multiple trials are required using different initial models to prevent being trapped into

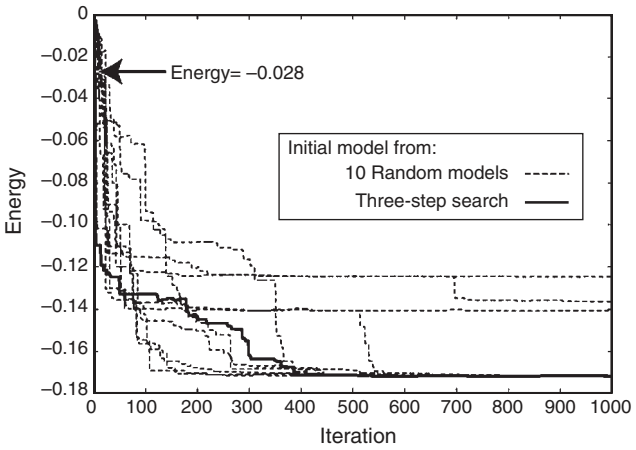

Fig. 6. Energy convergence in the SA search for different initial models. Dotted lines show the energy convergence from 10 randomly created initial models. The solid line shows the energy convergence from an initial model determined from the three-step search algorithm. The array indicates $E = -0.028$ which is the value obtained after application of the three-step search algorithm.

local minima. This greatly increases computation time. The result using the three-step search model as an initial model showed rapid convergence to a global minimum (solid line in Figure 6). This suggests that multiple trials might be avoided by using the initial model from the three-step search, thus increasing computational efficiency. Note that in this case the SA result is slightly dependent on the three-step search. The dependency can be reduced by using a wider search range for the CRS parameters.

Temperature functions in SA optimisation

The influence of temperature functions and number of iterations on the SA search are evaluated by applying SA to two ZO points; ZO point A (CMP 77 and two-way time = 0.802 s) and B (CMP 122 and two-way time = 0.684 s) using three exponential temperature functions (Figure 7*a*). The temperature functions we used to test energy convergence during the SA search were (T_0, C) = (0.001, 0.75), (0.003, 0.50), and (0.020, 0.50). Larger values of C give faster cooling rates.

The energy convergence plots for different temperature functions at the ZO point A (Figure 7*b*) show that for two temperature functions the energy converges towards a value around −0.170. However, it is slower for the temperature function with the highest initial temperature, (T_0, C) = (0.020, 0.50). Furthermore, for the temperature function with the fastest cooling rate, (T_0, C) = (0.001, 0.75), the energy is trapped at a local minimum around −0.14 after 300 iterations. Similarly, the convergence plots at ZO point B (Figure 7*c*) show that, for each temperature function, the energy converges towards a value around −0.162. However, for the temperature function with the highest initial temperature, (T_0, C) = (0.020, 0.50), convergence after 1000 iterations is incomplete.

The energy convergence at different ZO points shows different characteristics because the sequence of model parameters we obtain during the SA search depends on the initial model and the temperature function we use. If the initial model is close to the global solution, energy convergence should be fast, a faster cooling rate can be used, and computational cost will be moderate, but if the initial model is very different from the global solution, a slower cooling rate is required and computational cost will become higher.

Result of the CRS stack by SA

The temperature functions and number of iterations required for energy convergence should be different at different ZO points. However, we have assumed that the temperature function and the number of iterations determined by testing the subset of data (the two ZO points described above) do represent the optimal values for all ZO points. For our application of SA to all ZO points, we used the temperature function (T_0, C) = (0.003, 0.50), which showed a relatively fast energy convergence without being trapped in local minima for both ZO points A and B. We applied SA to all ZO points using this temperature function and 250 values of temperature, updating the CRS parameters twice for each temperature to give 500 forward calculations. If information is available about the spatial variation of the reliability of the initial model, different temperature functions can be used to accommodate these differences.

The continuity of the signals in the CRS stacked section resulting from SA searching (Figure 8*a*) is greatly improved in comparison to that from the three-step search (Figure 5), as shown by the difference between coherence values achieved

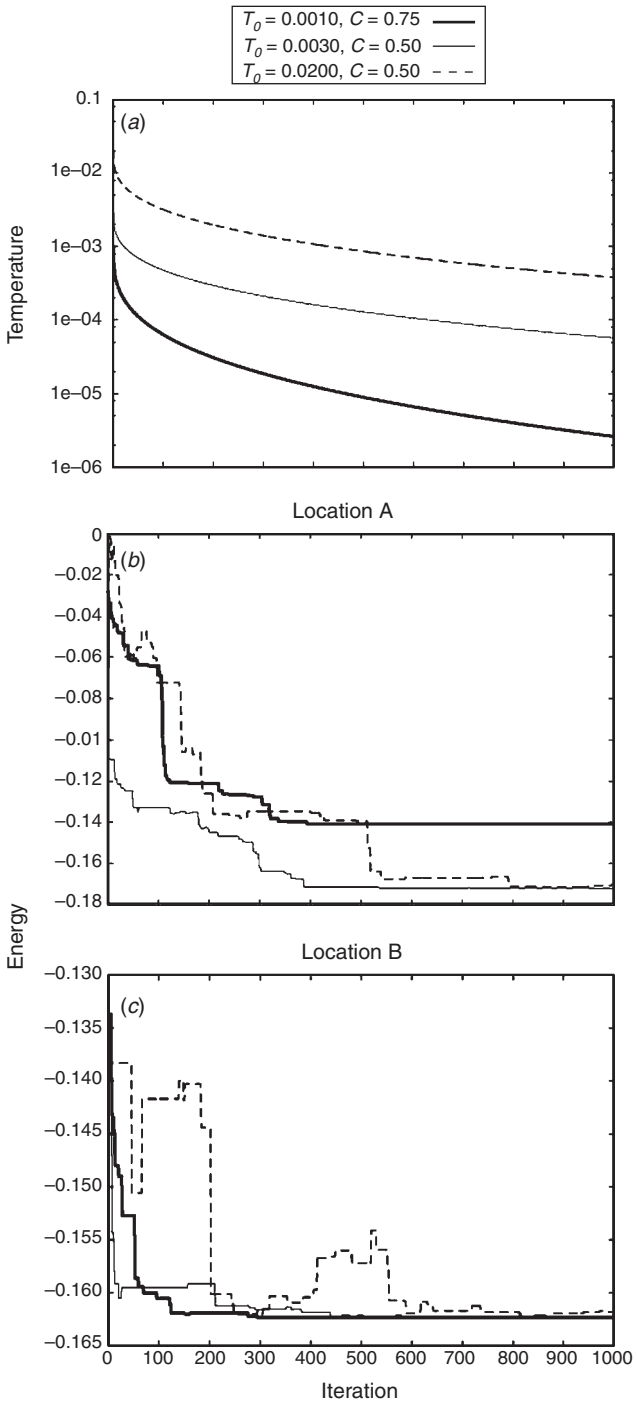

Fig. 7. Energy convergence in SA for three temperature functions for numerically modelled data. (*a*) The SA temperature functions (cooling schedules) used. (*b*) Energy convergence for each temperature function at location A of Figure 5 (CMP 77, two-way time = 0.802 s). (*c*) Energy convergence for each temperature function at location B of Figure 5 (CMP 122, two-way time = 0.684 s).

by the two approaches (Figure 8*b*). The coherence at some ZO points was up to 0.2 higher for the CRS stack by SA.

When we have true information about the subsurface (velocities and the shape of reflector), the CRS parameters can be analytically determined (e.g. Jäger, 1999). We have calculated the true CRS parameters by this method, and compare them with those from the initial three-step search model and the final SA search model in Figure 9. One can clearly see that the three-step search algorithm did not find the true model, and the SA search

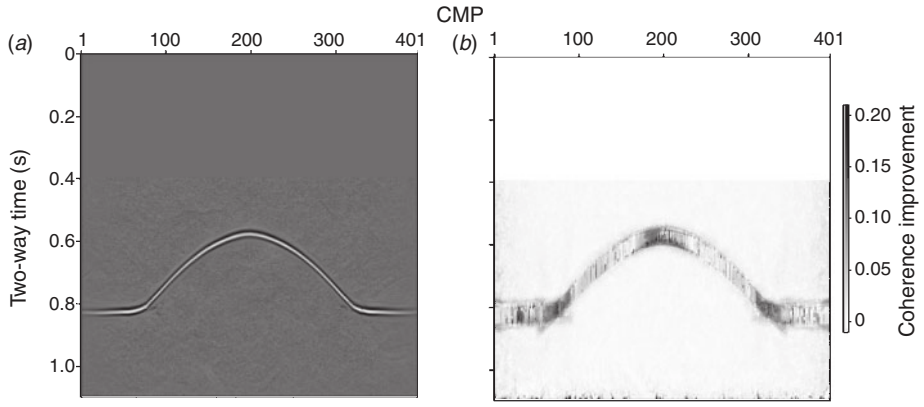

Fig. 8. (*a*) CRS stacked section for numerical model data, after optimisation by SA. (*b*) Coherence improvement achieved by using the SA search method with an initial model obtained by three-step search.

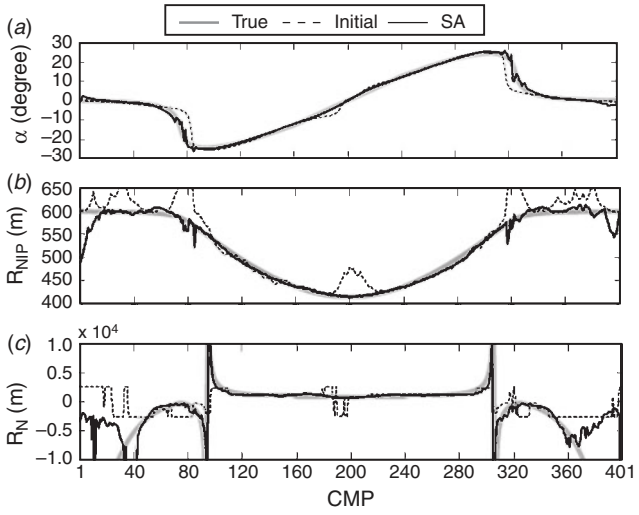

Fig. 9. CRS parameters (α, R_{NIP}, R_N) calculated from the true model, and estimated by the three-step search method, and by the SA search method.

algorithm did determine the CRS parameters more accurately (Figure 9).

Application to field data

Geological setting and seismic data

The Japanese Islands lie on a continental plate margin where the Philippine Sea plate is obliquely subducting beneath the Eurasian plate (Figure 10*a*). Our study area is in the Seto Inland Sea, which lies between Honshu and Shikoku Islands (Figure 10*b*). The area is characterised by an along-arc zonal arrangement of several geologic belts (Figure 10*a*). The Median Tectonic Line (MTL), which is the most significant geological boundary fault in Japan, passes through the study area, trending approximately parallel to the plate boundary. The western segment of the MTL is an active right-lateral strike-slip fault that separates low-pressure and high-temperature Ryoke metamorphic rocks to its north from high-pressure and low-temperature Sambagawa metamorphic rocks to its south (Figure 10*a*).

Crustal structures related to the MTL have been investigated by several authors using seismic reflection surveys (e.g. Ito et al., 1996; Kawamura et al., 2003; Ito et al., 2009). Although reflection profiles using conventional NMO stacking methods

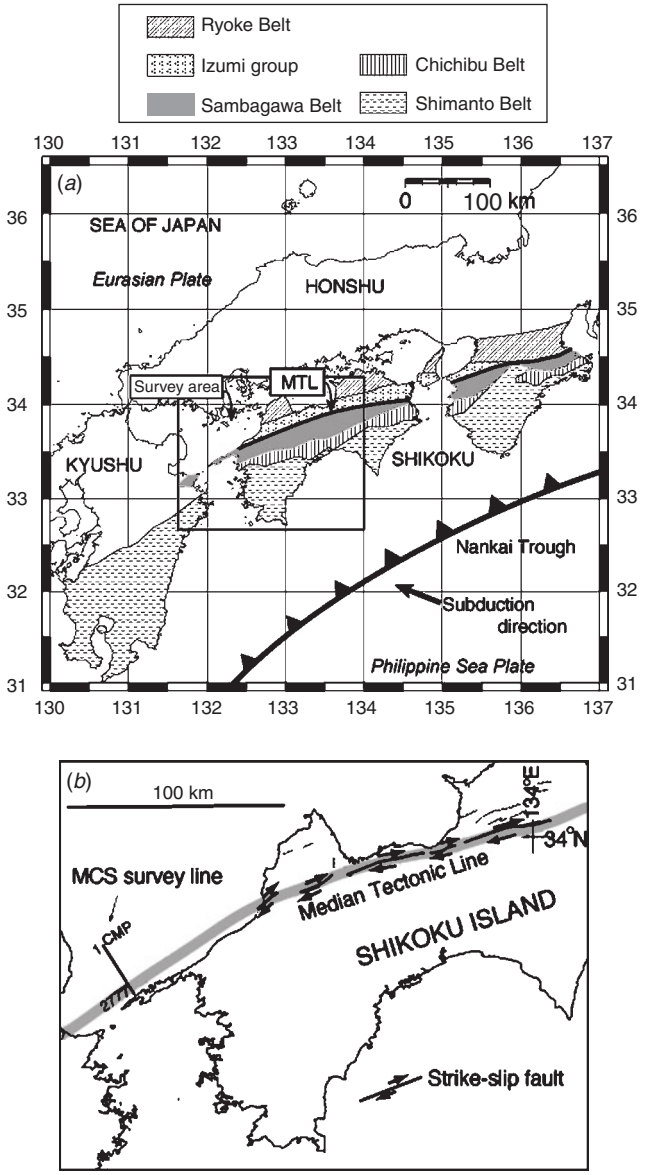

Fig. 10. (*a*) Simplified regional geologic map of southwestern Japan (modified from Wallis, 1998). The rectangle indicates the area shown in panel (*b*). (*b*) MTL and major strike-slip faults in the region near the seismic survey line of this study (modified from Kamata and Kodama, 1999). The survey line is indicated.

have identified a reflection that is believed to represent the MTL, the low fold gives rise to profiles with low SNR. To show the ability of the CRS stack method to provide reflection profiles with higher SNR than can be produced by conventional NMO stacking, we processed a 17-km-long multi-channel seismic (MCS) dataset acquired across and perpendicular to the MTL (Figure 10*b*). The acquisition parameters are summarised in Table 2. Ship traffic in the area between the islands restricted the length of the streamer we could tow, so the maximum fold was 12.

Conventional NMO stack processing

The pre-processing for NMO stacking included: first-break muting, bandpass filtering, amplitude recovery, and CMP sorting (Figure 11). Velocity analysis was performed at 1 km intervals. Following NMO correction with 30% stretch muting, we applied τ - p deconvolution to suppress multiple reflections, and used the interpolated velocity structure (V_{stack}) to produce a conventional NMO stacked section (Figure 12*a*). The section shows sub-horizontally layered Neogene-Quaternary sediments (Figure 12*b*) overlying a steeply dipping reflector observed between CMPs 2200 and 2700 that represents the top of the Sambagawa metamorphic rocks. The irregularly shaped reflector beneath the layered Neogene-Quaternary sequence marks the top of the Ryoke granitic rocks. The MTL could be identified with the active faults that cut Neogene-Quaternary sediments above the Sambagawa metamorphic rocks and it is believed to continue as the boundary between Ryoke metamorphic rocks and Sambagawa metamorphic rocks at depth.

Table 2. Acquisition parameters for the field data.

Number of shots	683
Shot interval	25 m
Number of receivers	48
Receiver interval	12.5 m
Number of CMPs	2777
CMP interval	6.25 m
Minimum/Maximum offset	75 m/662.5 m
Maximum fold	12
Record length for processing	3 s
Sampling rate	1 ms

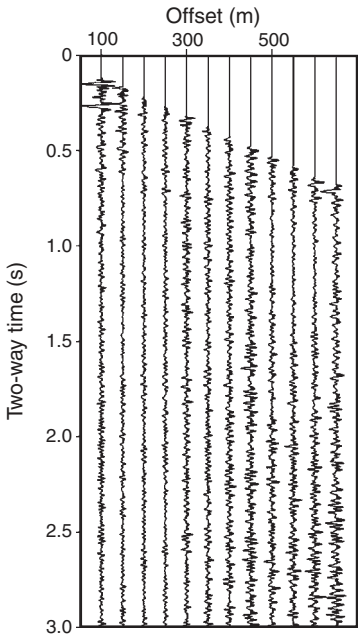

Fig. 11. 12-fold CMP gather from the field data at CMP 1251.

CRS stack processing

We applied the CRS stack to CMP gathers and used the three-step search to obtain initial models for the SA search algorithm.

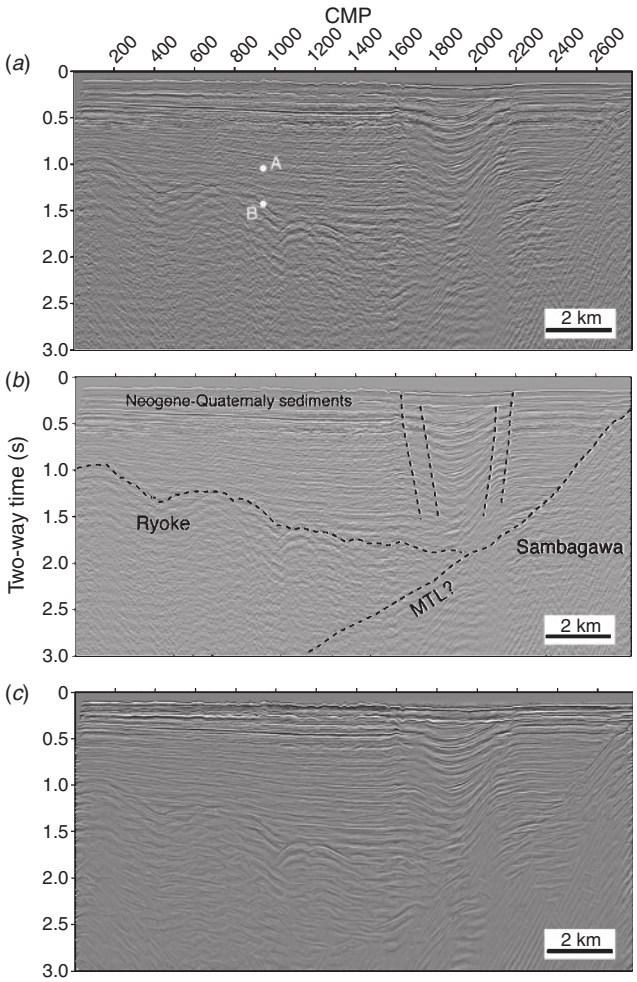

Fig. 12. Comparison of stacked sections: (*a*) NMO stack, (*b*) NMO stack showing interpreted boundaries and faults, and (*c*) CRS stack produced by conventional three-step parameter search.

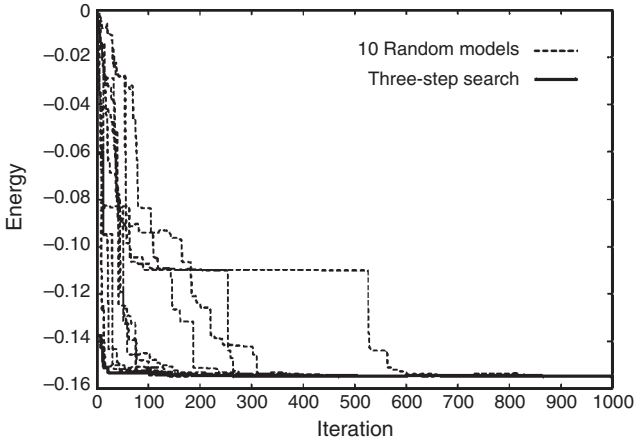

Fig. 13. Energy convergence for different initial models, at point B in Figure 12*a*.

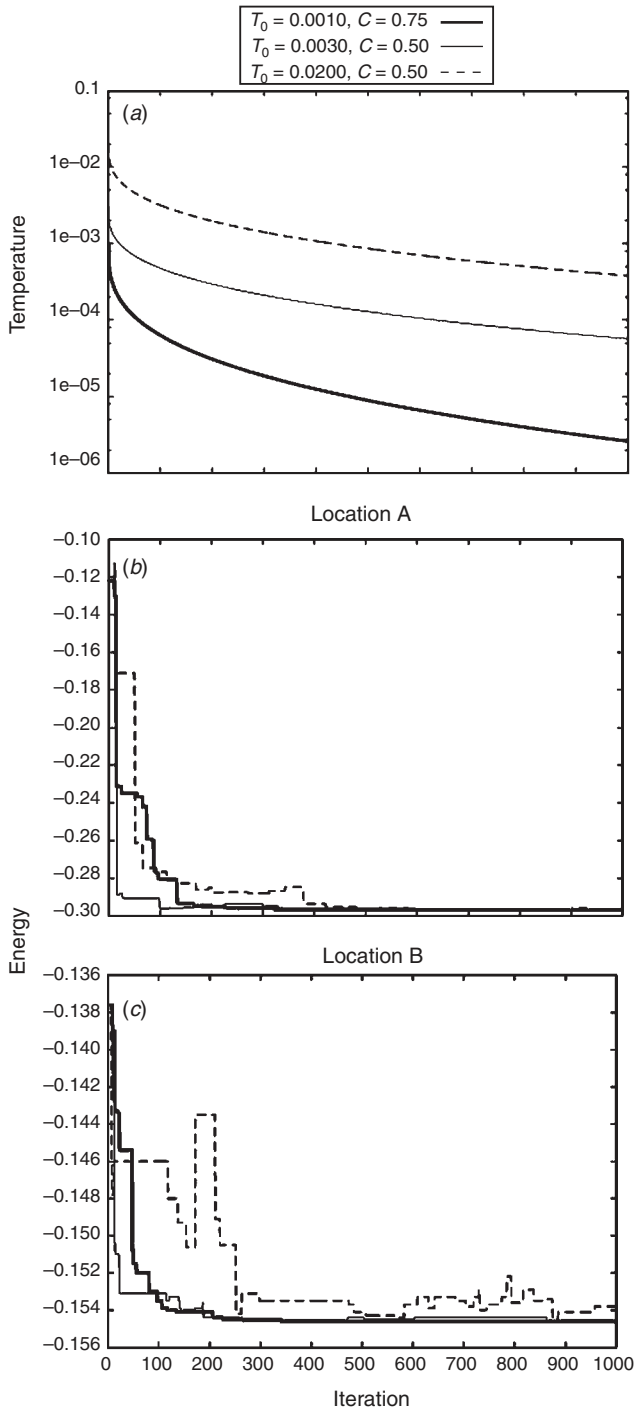

Fig. 14. Energy convergence in SA for three temperature functions for the field data. (*a*) The SA temperature functions (cooling schedule) used. (*b*) Energy convergence for each temperature function at location A of Figure 12 (CMP 950, two-way time = 0.944 s). (*c*) Energy convergence for each temperature function at location B of Figure 12 (CMP 950, two-way time = 1.460 s).

The search range for stacking velocity for the automatic CMP stack was based on the velocity model from the conventional velocity analysis used for the NMO stack. We designed a linearly interpolated search range within ± 200 m/s of the initial velocity model at 1.0 s two-way time and ± 600 m/s at 2.0 s two-way time. We applied linear ZO stacking to search for optimum emergence angles α within the range −30° to +30°, with a 0.5-degree step size. R_{NIP} was estimated from equation 3, and the search for R_N was done by using hyperbolic ZO stacking.

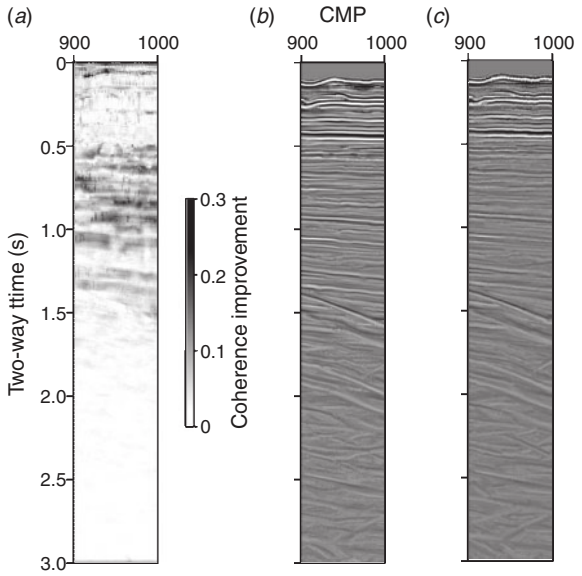

Fig. 15. (*a*) Coherence improvement for CMPs 900–1000 achieved by using the SA method with initial models obtained by a three-step search. (*b*) CRS stacked section after optimisation by SA. (*c*) CRS stacked section after three-step search.

For the ZO stacks and subsequent CRS stacking, we used a ZO aperture that was linearly interpolated from 50 m at 0.1 s to 200 m at 1.7 s. The CRS parameters obtained were then used to produce the CRS stacked section according to equation 1. The reflection events on the CRS stacked section produced by this conventional three-step parameter search (Figure 12*c*) show clear improvement over the NMO stacked section (Figure 12*a*); for example, the high-frequency noise has decreased in Figure 12*c*.

For our application of SA, we used the search ranges for α and γ (equation 13) of −30° to +30° and −90° to +90°, respectively. The search range for R_{NIP} was constrained to be within ± 50 m/s of the stacking velocity obtained from automatic CMP stacking at 1.0 s two-way time and within ± 300 m/s at 2.5 s. These constraints correspond to 10% of the reference velocity model.

We compared the energy convergence in the SA search at ZO point B (Figure 12*a*; CMP 950, two-way time = 1.46 s) by using 10 randomly created initial models and the initial model obtained from three-step search (Figure 13). Here, we used the temperature function (T_0, C) = (0.003, 0.50) in equation 10, substituting DIM = 3, using 500 values of temperature, and updating the CRS parameters twice for each temperature, giving 1000 forward calculations. All of the random models showed slower convergence than the three-step search model, as was the case for our application of SA to the numerical model (Figure 6), so we chose to use the initial models from the three-step search in the final processing effort.

We determined the temperature function and number of iterations for SA by testing a subset of the data (as we did for our numerical modelling experiment). We tested SA at ZO points A (Figure 12*a*; a region of sub-horizontal layering at CMP 950, two-way time = 0.944 s) and B (a region of dipping structure; CMP 950, two-way time = 1.46 s). We applied the same three temperature functions that were used in the numerical modelling experiment and showed that convergence after 1000 iterations for the function with a large initial temperature was inferior to that for the other two functions (Figure 14*b* and 14*c*). The energy of the fastest cooling rate

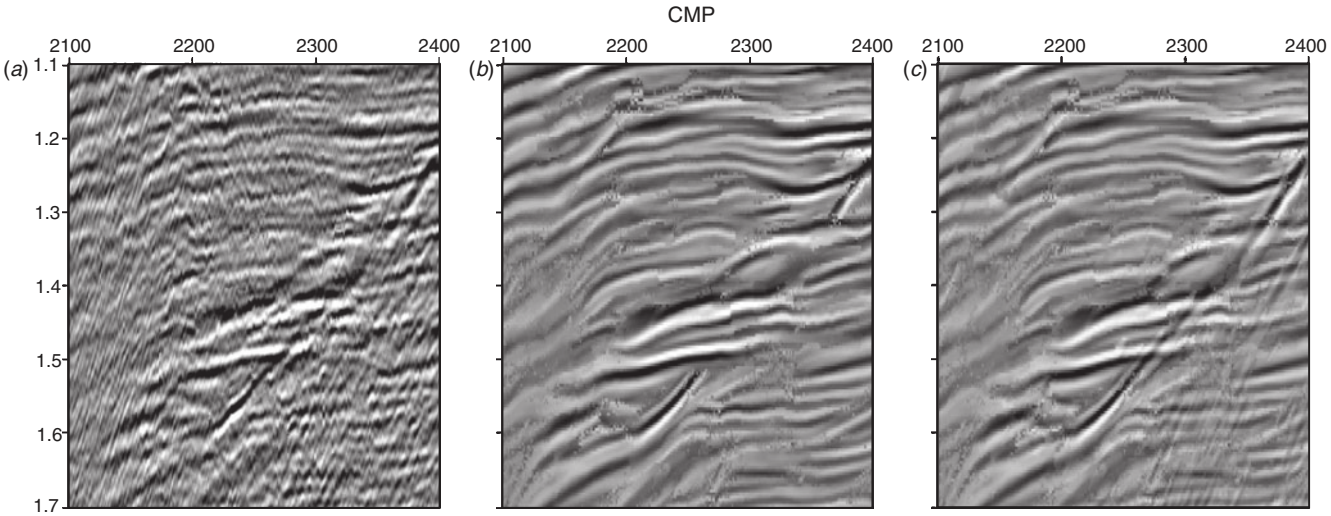

Fig. 16. Close-up of the stacked sections in the region of conflicting dip. (*a*) NMO stack, (*b*) CRS stack after global optimisation by SA, and (*c*) CRS stack after correction for conflicting dips.

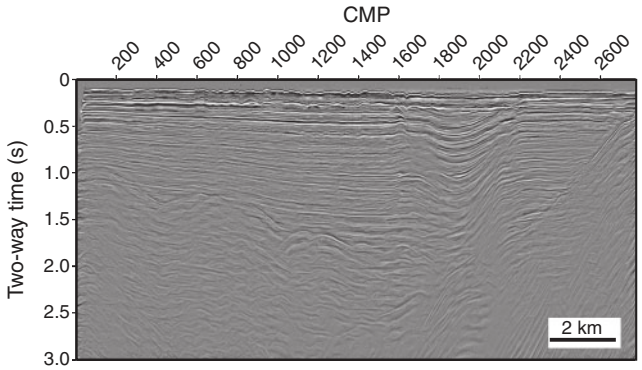

Fig. 17. CRS stacked section for field data with SA optimisation and correction for conflicting dips.

was not trapped in a local minimum, as had happened in the numerical modelling experiment. Using the temperature function with the slowest cooling rate would allow us to search a wider model space, which agrees with the result of the numerical modelling experiment.

We applied SA to the pre-processed CMP data (CMP 900–1000) using the temperature function (T_0, C) = (0.003, 0.50) and 250 values of temperature, updating the CRS parameters twice for each temperature to give 500 forward calculations. The coherence of the CRS stacked section obtained by SA was higher than that of the initial model (Figure 15*a*). Comparison of the CRS stacked section with parameters found by SA search (Figure 15*b*) with that from the three-step search (Figure 15*c*) clearly shows that the former has better continuity, better resolves reflection boundaries, and shows some differences in the shape of reflection boundaries. The CRS stacked section with SA (Figure 15*b*) does contain some high-frequency noise. This could be because the search range for R_{NIP} (calculated from the NMO stacking velocity) did not cover the optimum solution at some locations; this could be overcome by using a wider search range for R_{NIP}. However, this would also increase the number of iterations required for energy convergence and may also increase interference by multiple reflections.

We then applied the same temperature function and number of iterations to the entire seismic data. To reduce computation time, we applied the SA search method at 4 ms intervals (original data was sampled at 1 ms) and interpolated between SA results to simulate the original 1 ms sample rate. Therefore we performed 3D optimisations 2 085 527 times (2777 CMPs multiplied by 751 time samples). It took 30 h using an Intel Core i7 (2.93GHZ) CPU with 8-threaded code. We believe this is a quite reasonable computation time to obtain high SNR.

We then examined the NMO stacked section and the CRS stacked section with SA between CMPs 2100 and 2400 and two-way time from 1.1s to 1.7 s (Figure 16). These data show that the presence of apparent conflicting dips, attributed to diffraction events, causes suppression of the steeply dipping reflection events in the CRS stacked section (compare Figure 16*a* and 16*b*) (Müller, 2009). The method proposed to correct for this is to estimate the local solution of α in the linear ZO stack and then re-apply the three-step search with fixed α. The conflicting dips are then corrected by summing the global and local solutions of the CRS stacked section (Mann, 2002; Müller, 2009). Note that Müller (2009) searched for the local solution in a ZO section produced by the path-summation technique. We corrected the effect by applying a SA search using a fixed α for the local solution to the linear ZO stack. Figure 16*c* shows the CRS stacked section that represents the sum of the stack using global optimisation by SA and the stack using local optimisation by SA with fixed α, which is the first local minimum in the linear ZO stack.

The final CRS stacked section after correcting for conflicting dips (Figure 17) shows a clearer, better-resolved reflection image than that from either the conventional NMO stack and the CRS stack from three-step search. Thus CRS processing will help us to understand the detailed subsurface geological structure around the MTL and other faults.

Conclusions

We have shown an effective workflow for the estimation of the optimal parameters for CRS stacking, using a simulated annealing search scheme. SA searches using randomly created initial models required multiple trials with different initial models to prevent trapping in local minima. To overcome this problem, we propose the use of initial models determined from a three-step parameter search process, as we found that these initial models gave rapid convergence to a global solution in

the SA search step. This choice avoids multiple trials and increases computational efficiency.

We applied the SA search method to field data acquired across the MTL of south-western Japan. As our seismic data showed apparent conflicting dips, we corrected for this by applying local optimisation by SA search with fixed emergence angles found in the three-step search. The result provided considerable improvements in coherence and SNR over conventionally processed seismic reflection profiles. This CRS processing method will help us to understand the detailed subsurface geological structure around the MTL and other faults.

Acknowledgements

The authors thank Naoshi Aoki of JGI Inc. and an anonymous reviewer for constructive comments and discussions. S. Minato is grateful for the support of Grant-in-Aid for Japan Society for the Promotion of Science Fellows (212666). This study was supported by the Global Center for Education and Research on Human Security for Asian Megacities (GCOE).

References

Baykulov, M., and Gajewski, D., 2009, Prestack seismic data enhancement with partial common-reflection-surface (CRS) stack: *Geophysics*, **74**, V49–V58. doi:10.1190/1.3106182

Bergler, S., Hubral, P., Marchetti, P., Cristini, A., and Cardone, G., 2002, 3D common-reflection-surface stack and kinematic wavefield attributes: *The Leading Edge*, **21**, 1010–1015. doi:10.1190/1.1518438

Bonomi, E., Cristini, A. M., Theis, D., and Marchetti, P., 2009, 3D CRS analysis: a data-driven optimization for the simultaneous estimate of the eight parameters: *SEG Technical Program Expanded Abstracts*, **28**, 3284–3291. doi:10.1190/1.3255542

Duveneck, E., 2004, Velocity model estimation with data-derived wavefront attributes: *Geophysics*, **69**, 265–274. doi:10.1190/1.1649394

Garabito, G., Cruz, J., Hubral, P., and Costa, J., 2001, Common reflection surface stack: a new parameter search strategy by global optimization*SEG Technical Program Expanded Abstracts*, **20**, 2009–2012. doi:10.1190/1.1816536

Garabito, G., Cruz, J., Hubral, P., and Costa, J., 2006, Application of SA and VFSA global optimization algorithms for search of the 2-D CRS stacking parameters: *Wave Inversion Technology Consortium Annual Report*, **10**, 24–31.

Garabito, G., Cruz, J., and Lucena, L., 2009, 2D CRS stack: the use of the stacking velocity as an 'a priori' information in the optimization of CRS parameters: *Wave Inversion Technology Consortium Annual Report*, **13**, 220–227.

Gelchinsky, B., 1989, Homeomorphic imaging in processing and interpretation of seismic data (fundamentals and schemes): *SEG Technical Program Expanded Abstracts*, **8**, 983–988. doi:10.1190/1.1889838

Gelchinsky, B., Berkovitch, A., and Keydar, S., 1999, Multifocusing homeomorphic imaging: Part 1. Basic concepts and formulas: *Journal of Applied Geophysics*, **42**, 229–242. doi:10.1016/S0926-9851(99)00038-5

Höcht, G., de Bazelaire, E., Majer, P., and Hubral, P., 1999, Seismics and optics: hyperbolae and curvatures: *Journal of Applied Geophysics*, **42**, 261–281. doi:10.1016/S0926-9851(99)00040-3

Hubral, P., 1983, Computing true amplitude reflections in a laterally inhomogeneous earth: *Geophysics*, **48**, 1051–1062. doi:10.1190/1.1441528

Ingber, L., 1989, Very fast simulated re-annealing: *Mathematical and Computer Modelling*, **12**, 967–973. doi:10.1016/0895-7177(89)90202-1

Ito, T., Ikawa, T., Yamakita, S., and Maeda, T., 1996, Gently north-dipping Median Tectonic Line (MTL) revealed by recent seismic reflection studies, southwest Japan: *Tectonophysics*, **264**, 51–63. doi:10.1016/S0040-1951(96)00117-5

Ito, T., Kojima, Y., Kodaira, S., Sato, H., Kaneda, Y., Iwasaki, T., Kurashimo, E., Tsumura, N., Fujiwara, A., Miyauchi, T., Hirata, N., Harder, S., Miller, K., Murata, A., Yamakita, S., Onishi, M., Abe, S., Sato, T., and Ikawa, T., 2009, Crustal structure of southwest Japan, revealed by the integrated seismic experiment Southwest Japan 2002: *Tectonophysics*, **472**, 124–134. doi:10.1016/j.tecto.2008.05.013

Jäger, R., 1999, The common reflection surface stack - theory and application, Master' thesis, University of Karlsruhe.

Jäger, R., Mann, J., Höcht, G., and Hubral, P., 2001, Common-reflection-surface stack: image and attributes: *Geophysics*, **66**, 97–109. doi:10.1190/1.1444927

Kamata, H., and Kodama, K., 1999, Volcanic history and tectonics of the Southwest Japan Arc: *The Island Arc*, **8**, 393–403. doi:10.1046/j.1440-1738.1999.00241.x

Kawamura, T., Onishi, M., Kurashimo, E., Ikawa, T., and Ito, T., 2003, Deep seismic reflection experiment using a dense receiver and sparse shot technique for imaging the deep structure of the Median Tectonic Line (MTL) in east Shikoku, Japan: *Earth, Planets, and Space*, **55**, 549–557.

Kirkpatrick, S., Gelatt, C., and Vecchi, M., 1983, Optimization by simulated annealing: *Science*, **220**, 671–680. doi:10.1126/science.220.4598.671

Mann, J., 2002, Extensions and applications of the common-reflection-surface stack method, PhD thesis, University of Karlsruhe.

Menyoli, E., Gajewski, D., and Hübscher, C., 2004, Imaging of complex basin structures with the common reflection surface (CRS) stack method: *Geophysical Journal International*, **157**, 1206–1216. doi:10.1111/j.1365-246X.2004.02268.x

Müller, T., 1999, The common reflection surface stack method: seismic imaging without explicit knowledge of the velocity model, PhD thesis, University of Karlsruhe.

Müller, N., 2003, The 3D common-reflection-surface stack: theory and application, PhD thesis, University of Karlsruhe.

Müller, N., 2009, Treatment of conflicting dips in the 3D common-reflection-surface stack: *Geophysical Prospecting*, **57**, 981–995. doi:10.1111/j.1365-2478.2009.00803.x

Neidell, N. S., and Taner, M. T., 1971, Semblance and other coherency measures for multichannel data: *Geophysics*, **36**, 482–497. doi:10.1190/1.1440186

Nelder, J. A., and Mead, R., 1965, A simplex method for function minimization: *The Computer Journal*, **7**, 308–313.

Rothman, D. H., 1985, Nonlinear inversion, statistical mechanics, and residual statics estimation: *Geophysics*, **50**, 2784–2796. doi:10.1190/1.1441899

Sen, M. K., and Stoffa, P. L., 1995, *Global optimization method in geophysical inversion*: Elsevier Science B. V.

Thore, P. D., de Bazelaire, E., and Rays, M. P., 1994, The three-parameter equation: an efficient tool to enhance the stack: *Geophysics*, **59**, 297–308. doi:10.1190/1.1443592

Trappe, H., Gierse, G., and Pruessmann, J., 2001, Case studies show potential of common reflection surface stack: structural resolution in the time domain beyond the conventional NMO/DMO stack. Special topic: seismic processing: *First Break*, **19**, 625–633.

Velis, D. R., and Ulrych, T. J., 1996, Simulated annealing wavelet estimation via fourth-order cumulant matching: *Geophysics*, **61**, 1939–1948. doi:10.1190/1.1444109

Wallis, S., 1998, Exhuming the Sanbagawa metamorphic belt: the importance of tectonic discontinuities: *Journal of Metamorphic Geology*, **16**, 83–95. doi:10.1111/j.1525-1314.1998.00072.x

Yoon, M., Baykulov, M., Dümmong, S., Brink, H., and Gajewski, D., 2009, Reprocessing of deep seismic reflection data from the North German Basin with the Common Reflection Surface stack: *Tectonophysics*, **472**, 273–283. doi:10.1016/j.tecto.2008.05.010